Impact of Resolution on the Representation of the Mean and Extreme Winds along Nares Strait

G. W. K. Moore[1] and A. A. Imrit[1]

[1]University of Toronto

November 24, 2022

Abstract

Nares Strait is the long and narrow strait bounded by steep topography that connects the Arctic Ocean's Lincoln Sea to the North Atlantic's Baffin Bay. The winds that blow along the strait play an important role in modulating ice and water exports from the Arctic Ocean as well as in helping to establish the Arctic's largest and most productive polynya that forms at its southern terminus. However, its remote location has limited our knowledge of the winds along the strait. Here we use weather station data from the region as well as 3 numerical models with horizontal resolutions that vary from ˜30km to ˜2.5 km to characterize the wind field in the vicinity of the strait. The strait has a width that varies from ˜40km to ˜100 km and as such the wind field is typically ageostrophic and controlled by the pressure gradient in the along-strait direction. We show that model resolution plays a role in the representation of both the mean and extreme winds along the strait through the ability to represent this ageostrophic flow. Higher windspeeds occur in the vicinity of Smith Sound and are the result of a left-hand corner jet. Kane Basin, the widest section of the strait, is characterized by a pronounced zonal windspeed gradient that is the result of the steep topography of the upstream Washington Land peninsula.

Impact of Resolution on the Representation of the Mean and Extreme Winds along Nares Strait

G.W.K. Moore[1,2] and A.A. Imrit[3]

[1]Department of Physics, University of Toronto

[2]Department of Chemical and Physical Sciences, University of Toronto Mississauga.

[3]Department of Mechanical Engineering, University of Toronto.

Corresponding author: G.W.K. Moore (gwk.moore@utoronto.ca)

Key Points:

- The winds along Nares Strait play an important role in Arctic sea ice export as well as in the formation of the North Water Polynya.
- The strait is narrow with steep topography on either side and as a result, the ageostrophic processes play an role its wind climate.
- Model resolution plays a role in the representation of the ageostrophic mean and extreme winds along the strait.

Abstract

Nares Strait is the long and narrow strait bounded by steep topography that connects the Arctic Ocean's Lincoln Sea to the North Atlantic's Baffin Bay. The winds that blow along the strait play an important role in modulating ice and water exports from the Arctic Ocean as well as in helping to establish the Arctic's largest and most productive polynya that forms at its southern terminus. However, its remote location has limited our knowledge of the winds along the strait. Here we use weather station data from the region as well as 3 numerical models with horizontal resolutions that vary from ~30km to ~2.5 km to characterize the wind field in the vicinity of the strait. The strait has a width that varies from ~40km to ~100 km and as such the wind field is typically ageostrophic and controlled by the pressure gradient in the along-strait direction. We show that model resolution plays a role in the representation of both the mean and extreme winds along the strait through the ability to represent this ageostrophic flow. Higher windspeeds occur in the vicinity of Smith Sound and are the result of a left-hand corner jet. Kane Basin, the widest section of the strait, is characterized by a pronounced zonal windspeed gradient that is the result of the steep topography of the upstream Washington Land peninsula.

1 Introduction

1.1 The Role of Nares Strait in the Climate System

Situated between Greenland and Ellesmere Island, Nares Strait is the ~600km long and ~40-100km wide waterway that connects the Lincoln Sea to northern Baffin Bay (Figure 1). The strait is bounded by high topography on both the Greenland and Ellesmere Island sides. The Last Ice Area, that contains the Arctic's oldest and thickest sea ice, is situated to the north of Nares Strait (Moore et al., 2019). Nares Strait is an important pathway for the export of this important ice class out of the Arctic (Kwok et al., 2010). The wind field along Nares Strait with its preference for northly flow (Samelson et al., 2006) results in southward ice transport along the strait (Kwok et al., 2010; Moore et al., 2021). There is however evidence of periods where there is a reversal in ice motion with transport towards the north (Nutt, 1966; Kwok et al., 2010; Moore et al., 2021). There is also evidence of an increase in the ice export along Nares Strait over the past 20 years (Moore et al., 2021).

Ice arches that form most winters along the strait, at either its northern or southern end, can result in the cessation of this ice transport for months at a time (Kwok et al., 2010; Moore et al., 2021). There have been two recent winters, 2006/2007 and 2018/2019, when no arches formed along the strait (Kwok et al., 2010; Moore et al., 2021). In addition, there has been a reduction in the duration of ice arch formation since the late 1990s (Moore et al., 2021). The presence of these arches also contributes to the largest and most productive polynya in the Arctic, the North Water (NOW) that forms at the southern end of Nares Strait, in the vicinity of Smith Sound (Ingram et al., 2002). With an arch present, the northerly flow down Nares Strait, that accelerates in the exit region of Smith Sound, is able to remove sea ice thus contributing to the maintenance of the open water of the polynya (Barber et al., 2001).

Nares Strait is also an important pathway for the export of water from the Arctic Ocean to the North Atlantic Ocean (Jackson et al., 2014). The freshness of the surface waters of the Arctic Ocean implies that this export has the potential to impact the freshwater budget of the North Atlantic (Dickson et al., 1988) as well as the Atlantic Meridional Overturning Circulation (Dickson et al., 1996). The southward transport through Nares Strait also includes intermediate waters that originate in both the North Pacific and North Atlantic (Kozo, 1991; Jackson et al., 2014).

1.2 Observations of the Wind in the Vicinity of Nares Strait

Nares Strait is a remote location and as a result, there is still considerable uncertainty regarding the characteristics of the wind field in its vicinity. This uncertainty limits our ability to fully understand the role that winds along the strait play in ice and water export and in the formation of the NOW as well as the wind's role in the changes that are occurring in the region. Expeditions to the region during the late 19th century provide valuable information on the wind field that supplement modern observations.

Hayes (1867) overwintered at Cape Foulkes on the eastern side of Smith Sound (Figure 2) from September 1860 to July 1861. Bihourly meteorological measurements were made throughout the period including pressure and wind observations. A prevalence of northerly flow through Smith Sound was noted with a mean windspeed of approximately 9 ms^{-1}. Southerly flow was also noted although the windspeeds were typically lower. There were 25 storms, defined by windspeeds in excess of 22 ms^{-1}, during the 11 month stay with 19 of these events characterized by northerly flow. Several of the storms characterized by northerly flow were associated with pressure drops on the order of 13 mb. Steffen (1985) collected wind observations from Cape Sabine on the western side of Smith Sound from November 1974 to March 1976. While the mean windspeed was 8.7 ms^{-1} from the north, there were 14 events where the windspeed exceeded 20 ms^{-1} with the highest recorded windspeed being in excess of 40 ms^{-1}.

The United States North Polar Expedition's ship was trapped in ice at an exposed site in Hall Basin (Figure 2) during the winter of 1871/1872 (Bessels, 1876). The science party regularly observed windspeeds in excess of 20 ms^{-1} with a preference for northly flow. On storm in November 1871 was so severe that it was not possible to reach the anemometer during the most intense phase of the storm. The storm lasted for over 80 hours and the air temperature during the event fell from +1^{o}C to -18^{o}C, suggesting a reversal in wind direction from south to north. The winds were so strong that sea ice in Hall Basin and Robeson Channel was mobile (Bessels, 1876). In the vicinity of Robeson Channel (Figure 2), meteorological observations were made at Fort Conger from August 1881 to August 1883 during the First International Polar Year (Greely, 1888). The observations indicated the preference for bidirectional wind flow along Robeson Channel. There were numerous events where the windspeeds were in excess of 15 ms^{-1} (Greely, 1888).

An automatic weather station has been located on Hans Island, in the center of Kennedy Channel (Figure 2), since 2008 (Wilkinson et al., 2009) with data currently available from 2016-2019 (Moore, 2021). The observations indicate the flow is along the channel from either the north, the preferred direction, or from the south (Moore, 2021). Winds, with either direction, in excess of 30 ms^{-1} were observed. In agreement with earlier work (Samelson et al., 2006), northerly flow at Hans Island was associated with higher sea-level pressures over the Lincoln Sea as compared to northern Baffin Bay with the opposite being the case for southerly flow (Moore, 2021). Moore (2021) also noted that the winds at Hans Island were representative of the variability in the winds along much of Nares Strait.

The steep topography along the margins of the Greenland Ice Sheet (GrIS) can also lead to high winds resulting from katabatic flow (van As et al., 2015). These winds have been most extensively studied in southeast Greenland where the channeling of the katabatic flow through narrow fiords can lead to severe wind events known as Piteraqs (Oltmanns et al., 2014; Moore et al., 2016). The

GrIS also abuts Nares Strait (Figure 2) but there are few observations of wind events in the region. An exception is Thule (Fig 2) that has a long meteorological record associated with the airport operated by the United States Air Force. The record indicates that the site is one where high winds are common (Stansfield, 1972). A particularly intense event in March 1972 was associated with sustained winds from the southeast in excess of 30ms^{-1} and gusts in excess of 90 ms^{-1} (Stansfield, 1972). There is evidence that the event was the result of synoptic-scale flow interacting with steep local topography (Moore, 2016; Tollinger et al., 2019). The Petermann Glacier is a marine terminating glacier that flows into Hall Basin (Fig 2). It is a major outlet glacier and is estimated to drain approximately 6% of the GRiS (Falkner et al., 2011) It has a large floating ice tongue and winds that blow along the fiord may play a role in calving events (Falkner et al., 2011).

1.3 Representation of Winds in the Vicinity of Nares Strait in Numerical Models

The limited observations in the region indicate that Nares Strait is a region that is characterized by high winds. Indeed, Gutjahr and Heinnemann (2018) using a regional climate model identified Nares Strait, with 95th percentile 10 m windspeeds of 23 ms^{-1}, as one of the regions in the Arctic with the highest extreme winds. One of the reasons for these high winds is the channeling of the wind along the strait that is the result of the steep topography on both the Greenland and Ellesmere Island sides. This channeling is enhanced by the common occurrence of low-level temperature inversions in the region that serve to inhibit vertical motion (Kozo, 1991).

The narrowness of the strait and the steep topography along its sides requires high spatial resolution to represent it. Figure 2 shows the topography of the region as represented in the GEBCO digital elevation model (horizontal resolution ~0.5km), the ERA5 (horizontal resolution of ~30km), the ECOA (horizontal resolution ~9km) and the CARRA (horizontal resolution 2.5km). Please refer to the Data Section for additional information on the models used in this figure. As can be clearly seen, only the GEBCO and CARRA are able to capture the topography in the region including Nares Strait as a waterway connecting the Lincoln Sea to northern Baffin Bay. Both the ERA5 and the ECOA have difficulty representing the narrowest sections of the strait, Robeson and Kennedy Channels. The ECOA is able to represent some aspects of Kane Basin and Smith Sound.

In addition, the flow in such a long and narrow channel is typically ageostrophic (Overland, 1984) and as such, also requires high spatial resolution to represent it. Samelson and Barbour (2008) used the limited area numerical forecast model Polar MM5 (Bromwich et al., 2001) to generate a 2-year long climatology of the wind field along Nares Strait. The resolution of the inner domain was 6 km. The model was able to represent the bidirectional flow along the strait with the higher windspeeds being from the north. The model also had higher windspeeds in the narrower sections of the strait, Smith Sound and Kennedy Channel. The model was also able to represent the northerly winds in excess of 25 ms^{-1} that in April 2005 destroyed an ice camp established along the Kennedy Channel (Melling, 2011).

Moore and Våge (2018) compared the ability of 3 different model datasets, with horizontal resolutions that varied from 75km-9km, that were all based on the European Center for Medium Range Weather Forecasts's (ECMWF) Integrated Forecast System (IFS) to represent the air-sea interaction over the NOW. They found that increasing the model resolution resulted in an improvement in the representation of the kinematics of the flow in the vicinity of Smith Sound and the NOW. The impact of resolution on the thermodynamics and the air-sea heat fluxes was more nuanced. However, there was a doubling of the mean and a tripling of the extreme turbulent heat flux, the sum of the sensible and latent heat fluxes, over the NOW between the lowest and highest resolution models.

Kohnemann and Heinemann (2021) used the COSMO-CLM limted area climate model with a horizontal resolution of 15 km to represent the wind field along Nares Strait. The model was run for 30 winters from 1987/88 to 2016/2017. A comparison with observations at 4 sites in the region, Alert, Kitsissut, Qaanaaq and Thule (Figure 2), indicated root-mean-square errors on the order of 2 ms^{-1} and correlation coefficients that varied from 0.34 at Qaanaaq to 0.60 at Kitsissut. The highest mean windspeeds were found to occur just downstream of Smith Sound with a secondary maximum along Kennedy Channel.

Moore (2021) used automatic weather station data from Hans Island (Fig 2) located within Kennedy Channel to examine the impact that model resolution had on the representation of wind field along Nares Strait. Three different model datasets, with resolutions varying from 60km to 9km, that are all based on the ECMWF's IFS, were used. The root-mean square error decreased from 4.6ms^{-1} for the 60 km version to 4.1 ms^{-1} for the 30km version and then to 2.2 ms^{-1} for the 9 km version. The slope of the least squares fit of the model data to observations, a measure of the ability of the model to capture the magnitude of the winds, increased from 0.3 to 0.39 and then 0.8 with increasing model resolution. The correlation increased from 0.67 to 0.79 and then to 0.87. In addition, it was only the 9 km version that was able to capture the confinement of the high windspeeds to Kennedy Channel. Moore (2021) concluded that a model resolution of at least 9 km was required to represent the variability in the wind field along Nares Strait.

This paper extends previous work in two ways. First of all, data from 5 weather stations along Nares Strait (Fig 2) are used to assess the ability of models to represent the mean and extreme winds in the vicinity of the strait. In addition, the newly released Copernicus Arctic Regional Re-Analysis (CARRA) with a horizontal resolution of 2.5 km is included in the assessment.

2 Data

2.1 Observational Data

There are 5 weather stations in the region (Figure 2). Alert, operated by Environment and Climate Change Canada, is situated on the coast of the Lincoln Sea to the north of Nares Strait (82.5°N, 62.33°W). Hans Island, operated by the Scottish Association for Marine Sciences, is situated in the center of Kennedy Channel (80.82°N, 66.46°W). There are also two Greenlandic stations that are operated by the Danish Meteorological Institute: Kitsissut (76.63°N, 73°W) and Qaanaaq (77.48°N, 69.38°W). The United States Air Force also operates a station at Thule (76.53°N, 68.70°W). Typically data is available hourly but for this study, the data was subsampled to a 6-hourly frequency. The Hans Island data is only available from 2016-2019, with the exception of a an approximate 3 month period from May-July 2016, when there were intermittent reversals in the zonal wind component (Moore, 2021). This period was selected for the other locations as well so that the number of data points was approximately constant.

2.2 Model Data

In this paper, we will make use of 2 model datasets based on the ECMWF's IFS. Included is the new fifth generation reanalysis from the ECMWF or ERA5 with a horizontal resolution of ~30km and a temporal resolution of one hour (Hersbach et al., 2020) as well as the current version of their operational analysis or ECOA, with a horizontal resolution of ~9km and a temporal resolution of

6 hours (Holm et al., 2016). The ERA5 is based on Cycle 41r2 of the IFS. Being an operational product, the ECOA is based on a number of different cycles of the IFS from Cycle 41r2 up to Cycle47r1. The ECOA is available at this resolution from 2016 onwards. No material changes to the IFS, that would impact the present study, occurred over the period under consideration 2016-2019.

In addition, we will use the western domain, that encompasses Greenland, its surrounding seas as well as northern Ellesmere Island (Figure 1), of the Copernicus Arctic Regional Reanalysis (CARRA) with a horizontal resolution of 2.5 km and a temporal resolution of 3 hours (Yang, 2020). The CARRA is based on the non-hydrostatic mesoscale Numerical Weather Prediction (NWP) system known as HARMONIE-AROME (Bengtsson et al., 2017) with some modifications and extensions that are described in Yang (2020). Boundary conditions for CARRA are provided by the ERA5.

The ERA5 and ECOA have a common underlying model architecture and as a result contain the same parameterizations. The CARRA is a different model with a different data assimilation system and parameterizations. In addition the ERA5 and ECOA are hydrostatic, while the CARRA is non-hydrostatic. As a result, changes in the representation of the wind field between the models is not solely the result of changes in model resolution. It was felt that the availability of the CARRA with its high spatial resolution merited this tradeoff. A similar tradeoff has been used in other studies of topographic flow distortion in the vicinity of Greenland (Bromwich et al., 2015; Moore et al., 2015; Moore et al., 2016; Kohnemann & Heinemann, 2021).

To assess the ability of the models to represent the observed variability in the winds at the five sites, the 10m wind fields from the models were interpolated to their locations for the period 2016-2019. The 10m winds will be used as the models represent, to some degree, the topography in the vicinity of the weather stations. The exception is Hans Island which is a small isolated island with a height of approximately 170 m above sea-level. None of the models resolve the island and hence the 10m winds are biased low (Moore, 2021). For this reason, we will also compare the 100m winds at the Hans Island site.

The representation of the mean and extreme winds along the strait, we will also consider the period 2016-2019 so as to allow for inclusion of the ECOA in the comparison. The CARRA and ERA5 are both available for longer periods of time. It was found that the longer periods produced results consistent with the 2016-2019 period.

3 Results

3.1 Comparison with Observations

The statistics of the comparison between the observed 10m windspeeds from the ERA5, ECOA and CARRA are shown in Table 1. A slopesless than one indicates that the model underestimates the windspeeds and as can be seen, in all cases this is the case. However there is an increase in the slope with increasing model resolution, i.e. as one progresses from the ERA5 to the ECOA and then to the CARRA. With the CARRA slopes typically are on the order of 0.8 as compared to 0.44 for the ERA5. As a result, the CARRA has an improved representation of the windspeeds at the stations. The correlation coefficient, that is a measure of the amount of the variability in the observations captured in the model, also shows an increase with increasing model resolution. However the changes are more modest suggesting a degree of linearity between the observations and models. The root mean square and bias errors, measures of the spread between observations and models, also decreases with increasing model resolution.

There are some differences between the various locations. Generally, the impact of resolution is most pronounced in regions with significant local topography, such as Hans Island, Qaanaq and Thule, and less pronounced in regions where topographic influences are small, such as Alert and Kitissut. At Hans Island, there is a general improvement in the statistics when one considers the 100m winds as compared to the 10m winds. The exception is the root mean square errors that are uniformly larger at 100m as compared to 10m. This suggests that the improvement may be partly the result of the higher windspeeds at 100m that act to remove the underestimation of the high windspeeds that is a characteristic of all the models.

To provide some additional information on the representation of the winds along the strait, we present in Figure 3 and 4, the wind roses at Hans Island and Thule. These are locations where the impact of topography is most significant.

The observations at Hans Island (Fig 3a) indicate the flow is bidirectional along Kennedy Channel with a preference for northerly flow. However extreme events, windspeeds>20ms^{-1}, occur for both directions. ERA5 (Fig 3b) is able to represent the bidirectionality of the flow at Hans Island but, consistent with the results from Table 1, underestimates the occurrence of high windspeeds. The ECOA (Fig 3c) and CARRA (Fig 3d) both capture the bidirectionality and have an improved representation of the occurrence of high winds at Hans Island. However both underestimate the occurrence of high speed winds especially from the south.

The observations at Thule (Fig 4a) indicates a clear preference for easterly flow with evidence that the highest speed come from the southeast. The ERA5 (Fig 4b) and ECOA (Fig 4c) both have challenges with the directionality and, consistent with the results in Table 1, the magnitude of the winds. The CARRA (Fig 4d) captures the directionality, albeit with an error in the direction and also has an improved representation of the magnitude of the wind.

3.2 The Distribution of Mean and Extreme Winds in the vicinity of Nares Strait

Figure 5 compares the distribution of the mean and 95th percentile 10m windspeed in the vicinity of Nares Strait. All models have the highest mean and extreme windspeeds in the Smith Sound region with the two higher resolution models, ECOA and CARRA, having a secondary maxima along Kennedy and Robeson Channels. The highest 95th percentile 10m windspeeds in CARRA, in excess of 22 ms^{-1}, occur at three locations in the vicinity of Smith Sound. There are locations at the eastern and western limits of the sound as well as a location along the steep topography just to the east of the sound. The CARRA, and to a lesser extent the ECOA, have a pronounced east-west gradient in the mean and extreme windspeeds across Kane Basin. The lower windspeeds in the eastern section of the basin are most likely the result of sheltering by the high topography of the Washington Land peninsula (Fig 2). The ECOA also has higher mean and extreme windspeeds in in the western Kane Basin that is absent in the CARRA and ERA5.

All models also indicate that the GRiS is a region of high mean windspeeds with the ERA5 and ECOA having higher magnitudes as compared to the CARRA. Extreme windspeeds over the Greenland Ice Sheet are restricted to areas at the margin of the GrIS in the vicinity of northern Baffin Bay. The CARRA also has a region of high mean and extreme windspeeds along the margins of the GrIS in northwest Greenland in the vicinity of the Petermann Glacier that are not resolved by the ERA5 and ECOA. Over Ellesmere Island, there are a number of local maxima in the CARRA, again not resolved in the lower resolution models, that are associated with topographic features within the Prince of Wales Mountains, the Victoria and Albert Mountains and the British Empire Range. The maximum along the western boundary of the Prince of Wales Mountains is the most pronounced.

As noted in Figure 5, there are three regions in the vicinity of Smith Sound where the CARRA 95th percentile 10m windspeed was in excess of 23ms^{-1}. The western location is situated in the vicinity of the appropriately named Gale Point (78.2°N, 75.45°W) named by Inglefield in 1852 who visited Smith Sound during one of the searches for Sir John Franklin (Wright, 1940). Distinct events where the CARRA 10m windspeed in the western and eastern Smith Sound region exceeded this value were identified. The criteria that events had to be separated by at least 1 day was used. This resulted in 49 distinct events at the western location and 45 events at the eastern location during the period January 1 2016 to December 31 2019. The sea-level pressure, 10m wind and 10m windspeed from the ERA5, ECOA and CARRA for these events were averaged to generate a composite of the meteorological conditions associated with the extreme winds in the Smith Sound region. Results are shown in Figure 6.

Focusing on the western location (Fig 6a-c), the high winds in all three models can be seen to be associated with a pressure gradient along the Smith Sound that is the result of a low-pressure center to the southwest of Nares Strait. The along-strait pressure gradient is most resolved in the CARRA as is the associated ageostrophic flow that is largest just downstream of the narrowest section of Smith Sound. Farther downstream, there is a transition to geostrophic flow. In the CARRA and to a lesser extent in the ECOA, there is a secondary maxima in windspeed to the east of Smith Sound that is also associated with a localized pressure gradient. In the CARRA, there are similar secondary maxima to the west of Smith Sound. In all instances, these secondary maxima form in regions of steep local topography (Fig 2). The CARRA composite at the eastern location (Fig 6d), has a similar structure to that at the western location (Fig 6c). This includes a windspeed maximum in the vicinity of Gale Point. One of the only difference between the two composites is an enhanced pressure gradient to the east of Smith Sound.

3.3 Spatial Correlation of the 10m windspeeds in the vicinity of Nares Strait

One-point correlation maps are a way to characterize the spatial variability in a geophysical field (Wallace & Gutzler, 1981; De Benedetti & Moore, 2020). We apply this technique to assess the impact that model resolution has on the spatial scale over which the 10m windspeed field at various locations in the vicinity of Nares Strait is representative of winds along the strait. In addition to the spatial distribution of the correlation field, the 0.7, 0.8 and 0.9 correlation coefficient contours are shown. They delimit the areas where the variability in the 10m windspeed at the target location explain 49%, 64% and 81% of the variability in the 10m windspeed field (De Benedetti & Moore, 2020).

Figure 7 presents results for Alert, situated at the northern end of Nares Strait (Fig 2). The ERA5 one-point correlation map (Fig 7a) indicates a large region, that includes the Robeson Channel and the southern Lincoln Sea, over which the Alert 10m windspeed can explain at least 50% of the variability in the 10m windspeed field. Both the ECOA (Fig 7b) and CARRA (Fig 7c) have reduced areas of high correlation that do not overlap with Nares Strait but with a tail extending northwards over the Lincoln Sea.

Figure 8 presents the one-point correlation maps for Hans Island, situated in the middle of Nares Strait (Fig 2). For all three models, the region of enhanced correlation is aligned with the orientation of the Kennedy Channel. The ERA5 map (Fig 8a) has this region overlap the topography on either side of the channel. In contrast, the CARRA map (Fig 8c) and to a lesser extent, the ECOA map (Fig 8b) have the region of enhanced correlation limited to the strait itself with gradients in correlation along either side. In addition, the CARRA has localized regions of enhanced correlation that extend inland in the vicinity of fjords that flow into the Kennedy Channel (Fig 2). Unlike what occurred at Alert, the region with a correlation greater than 0.9 is approximately constant with resolution and extends along much of Kennedy Channel indicating that the wind field at Hans Island is representative of the flow along the extent of the channel.

In Figure 9, the one-point correlation maps for the western Smith Sound windspeed maxima near Gale Point are shown. For all three models, the area of elevated correlation is confined to the western section of northern Baffin Bay to the south of Gale Point. Across Smith Sound, all models indicate that the variability at Gale Point can explain at least 50% of the variability. As was the case for Hans Island, the area of elevated correlation is approximately constant as a function of resolution. As was also the case at Hans Island, the CARRA one-point correlation map includes fine-scale structure associated with the topography along the western side of Smith Sound.

4 Conclusions

Nares Strait is a long and narrow waterway that connects the Lincoln Sea to the northern Baffin Bay (Figure 1). As such, it represents an important conduit between the Arctic and North Atlantic Oceans. Indeed, the strait is an important pathway along which old and thick sea ice leaves the Arctic (Kwok et al., 2010; Moore et al., 2021). Currents along the strait also transport water from the Arctic Ocean southwards (Jackson et al., 2014). The Arctic's largest and most productive polynya, the NOW, is situated to southern end of Nares Strait (Ingram et al., 2002). The winds that blow along the strait play an important role in modulating these exports (Samelson et al., 2006) as well as in maintaining the NOW (Barber et al., 2001).

In this paper, 3 different models, the ERA5 reanalysis, the current operational analysis from the ECMWF (ECOA) as well as the Copernicus Arctic Regional Re-Analysis (CARRA), were used to characterize the mean and extreme winds in the vicinity of Nares Strait. The models have horizontal resolutions that vary from 30 km to 2.5 km. The narrowness of the strait, that varies from ~40km to ~100km, can pose a challenge for models to represent its topography. As shown in Figure 2, the ERA5 with a horizontal resolution of ~30km, and to a lesser extent the ECOA, with a horizontal resolution of ~9km, are unable to represent key characteristics of strait, including the existence of an open waterway that connects the Lincoln Sea and northern Baffin Bay as well as the steep topography that abuts the strait. It is only the CARRA, with a horizontal resolution of 2.5km, that is able to capture these characteristics.

The winds from these datasets were compared to 5 weather stations in the vicinity of the strait. As shown in Table 1, there is a steady improvement in the ability of the models to represent the variability in the wind field with increasing resolution. However, all models have a slope of the least-squares linear fit to the data that is less than one. This indicates that the models all underestimate the windspeed. Averaging over the 5 weather stations, this slope increases from 0.44 for the ERA5 to 0.63 for the ECOA to 0.8 for the CARRA. This implies that, on average the windspeeds in the ERA5 are ~40% of the observed values. In contrast, the CARRA windspeeds are ~80% of the observed values. The correlation coefficient between the model and observations has a more modest improvement with resolution increasing from 0.72 for the ERA5 to 0.77 for the ECOA to 0.83 for the CARRA. As a result, the ERA5 windspeeds explain ~50% of the variability in the observed winds, while the CARRA explains ~65% of this variability. In addition, there is a reduction in the both the root mean square and bias errors with increasing resolution. Wind roses at Hans Island confirm the ability of the models to represent the bidirectionality of the flow along Nares Strait (Fig 3). The Thule wind roses (Fig 4) indicate that all the models are challenged with representing the directionality of the observed flow with the CARRA performing best.

It should be noted that in regions of complex topography, it remains a challenge to reconcile station-level data with models as a result of small scale inhomogeneity that may not represented in point observations (Dulière et al., 2011). In this context, the improvement in the representation of the Hans Island observations with the 100m wind field as compared to the 10m wind field (Table 1) is an example. It is likely that this characteristic is at play at other sites. The exception being Kitsissut which is situated at 11m asl on an island in northern Baffin Bay (Fig 2). At this site, there is a more modest improvement in the representation of the wind field with resolution (Table 1). Given its open-ocean location, Kitisissut may represent the best-case scenario for representing the observed wind field with model data. In this context, it is clear that even for stations in regions of steep topography, it is only the CARRA that approaches this best-case scenario.

The spatial variability in the mean and 95th percentile 10m windspeeds (Fig 5) show an increase in detail with increasing model resolution. All models are able to capture the maxima in the mean 10m windspeed to the south of Smith Sound as well as a maxima over the GRiS. Over the GRiS, the mean 10m windspeeds in the ERA5 and ECOA are higher than in the CARRA. This is likely the result of differences in the parameterizations between the two underlying models, the IFS and HARMONIE-AROME. The ERA5 is unable to represent a local maxima in the mean windspeed along Kennedy Channel that is most likely the result of its inability to represent the waterway in this region (Fig 2a). In addition, the ECOA windspeeds in the exit region of the Kennedy Channel over northern Kane Basin are higher than those in the CARRA. This may also be the result of differences in model parameterizations. The ECOA and CARRA also have a gradient in the mean 10m windspeeds across Kane Basin that is most likely associated with the representation of the topography of the Washington Land peninsula situated to the north of the eastern Kane Basin. In addition, the CARRA has fine scale structure in the mean 10m windspeed over both Ellesmere Island as well as over Greenland. This is likely the result of the high spatial resolution of the model as compared to the ERA5 and ECOA as well as its non-hydrostatic nature.

The 95th percentile 10m windspeeds have a similar structure and dependence on model resolution as was the case for the mean 10m windspeed. Amongst the differences is a restriction of the maxima over the GRiS to the region to the east of northern Baffin Bay. There is evidence that extreme winds in this region are associated with extra-tropical cyclones over northern Baffin Bay (Moore, 2016) and their inability to move farther north maybe the cause for the more limited region of extreme windspeeds. The CARRA also has a maxima in the 95th percentile 10m windspeeds in the vicinity of the Petermann Glacier in northwest Greenland that may be associated with katabatic winds in the region that are accelerated by channeling as they flow down the fjord. High winds in this region have been suggested to be associated with calving events (Falkner et al., 2011). In addition, the CARRA has isolated maxima across Ellesmere Island that are tied to topographic features. The most pronounced is an extended maxima along 82^{o}W from 76^{o}N to 79^{o}N that is aligned with steep topography on the western limit of the Prince of Wales Mountains (Fig 2). The high winds in the region may be associated with downslope wind storms (Smith, 1985).

The highest 95th percentile windspeeds occur in the vicinity of Smith Sound where CARRA identified three regions; one at the western limit of the sound, one at the eastern limit of the sound as well as one associated with steep topography to the east of the sound, where they were in excess of 22 ms^{-1} (Fig 5f). Composites of the sea-level pressure, 10m windspeed and 10m winds for these events were calculated for each of the three models (Fig 6). The composites show that extreme winds in the Smith Sound region are associated with extra-tropical cyclone situated to the southeast. In the vicinity of Smith Sound, there is an along-strait pressure gradient with ageostrophic flow being responsible for the high windspeeds. Downstream over northern Baffin Bay, the flow becomes geostrophic. The representation of this along-strait pressure gradient improves increasing model resolution as do the highest 10m windspeeds that occur at the exit of Smith Sound. This is consistent with observations and models of gap flow in other parts of the world such as the Columbia Gorge in the Pacific Northwest (Sharp & Mass, 2004).

The CARRA captures isolated maxima in the composite 10m windspeed field along both the western and eastern regions of Smith Sound. The western maxima is more pronounced in the composite for both the western and eastern regions of Smith Sound (Fig 6c&d). This western maxima is associated with a small-scale trough in the sea-level pressure field that has a similar structure to that associated with the 'corner jets' that form downwind of Cape Tobin in southeast Greenland (Petersen et al., 2009; Moore et al., 2016) as well as Capes Navarin and Olyutorsky along the Siberian coast of the northern Bering Sea (Moore & Pickart, 2012). Corner jets are the result of ageostrophic acceleration to the left of the topographic barrier (Godske, 1957; Barstad & Grønås, 2005).

Heinemann (2018) used a research aircraft to observe gap flow in Smith Sound. Flights were made along strait to observed the structure of the flow during June 2010. The gap flow was shown to be associated with a low-level jet with a jet core at a height of 100-200m asl. Maximum windspeeds on the order of 40ms^{-1} occurred 20-50km downstream of Smith Sound. In the across-front direction there was evidence of higher windspeeds to the west of the sound's centerline that is consistent with the presence of the corner jet identified in this paper.

The one-point correlation maps of the 10m windspeed can be used to identify the spatial extent over which the wind field at a given point provided information on the variability in this field. Results for Alert (Fig 7) show a strong dependence with model resolution and indicate that data from this station is only weakly correlated (correlation less than 0.7) with winds along Nares Strait. In contrast, the one-point correlation maps for Hans Island (Fig 8) and for Gale Point (Fig 9), near the location of the Smith Sound corner jet, are similar in extent with changing resolution. The CARRA does however have finer-scale structure, related to topography, that is absent in the ERA5 and ECOA.

The results presented here are consistent with previous studies (Samelson & Barbour, 2008; Moore & Våge, 2018; Kohnemann & Heinemann, 2021; Moore, 2021) that indicate that the representation of the flow along Nares Strait requires models with sufficient horizontal resolution to represent the ageostrophic processes that are the result of the narrowness of the strait and the steep topography that abuts it on both the Ellesmere Island and Greenland sides. Consistent with the results of Moore (2021), the ERA5 with a horizontal resolution of ~30km is unable to represent the topography of the region (Fig 2) and underestimates both the mean and extreme wind conditions at the stations in the vicinity of the strait (Table 1 and Fig 3&4) as well as the wind field along the strait (Fig 5&6). There are also improvements in the representation of the wind climate in the vicinity of Nares Strait in the CARRA as compared to the ECOA. As demonstrated by the Alert one-point correlation map (Fig 7), proximity does not necessarily imply that a station's wind climate is representative of conditions along the strait. Sites situated within the strait itself, such as Hans Island (Fig 8), are more representative of conditions. This is presumably the result of the channeling of the wind along the strait that constrain the flow.

These results suggest that care must be taken when interpreting studies that use the ERA5 reanalysis to characterize the wind field's role in ice motion along the strait (Shokr et al., 2020; Kirillov et al., 2021). In particular, the ERA5's underestimation of both mean and extreme windspeeds along the strait is cause for concern as is its inability to represent features such as the gradient in windspeed across Kane Basin. Ice-ocean models of the Nares Strait region that are forced by atmospheric datasets with a resolution comparable to the ERA5 (Dumont et al., 2010; Grivault et al., 2018) may also have these biases.

Acknowledgments

The authors would like to acknowledge the support of the University of Toronto's Center for Global Change Science that supported AAI's participation in this research. GWKM would like to acknowledge support from the Natural Sciences and Engineering Research Council of Canada.

Open Research

Data from the Alert weather station is available from Environment and Climate Change Canada (https://climate.weather.gc.ca). Data from the Hans Island weather station is available from the Scottish Association for Marine Sciences (https://dataservices.sams.ac.uk/aws/). Data from the Kitsissut and Qaanaaq weather stations are available from the Danish Meteorological Institute (https://www.dmi.dk). Data from the Thule weather station is available from the National Oceanic and Atmospheric Administration (https://gis.ncdc.noaa.gov/maps/ncei/cdo/hourly). The ERA5 and CARRA data are available from the Copernicus Climate Store (https://cds.climate.copernicus.eu/). The ECOA data is available from the University Corporation for Atmospheric Research (https://rda.ucar.edu).

Figure Captions

Figure 1) Topography (km) from the western domain of the Copernicus Arctic Regional Reanalysis. The Nares Strait region is indicated by the white polygon. The locations of the Lincoln Sea (LS), Ellesmere Island (EI), Nares Strait (NS) and northern Baffin Bay (NBB) are indicated.

Figure 2) Topography (km) of the Nares Strait region as represented in the: a) GEBCO DEM; b) ERA5, c) ECOA and d) CARRA. In a) the abbreviations for locations along the strait are: northern Baffin Bay (NBB); Smith Sound (SS); Kennedy Channel (KC); Hall Basin (HB); Robeson Channel (RC), Washington Land (WL) and the Petermann Glacier (PG). Regions of high topography on Ellesmere Island, the Prince of William Mountains (PWM); the Victoria and

Albert Mountains (VAM) and the British Empire Range (BER) are indicated. In b)-d), the locations of AWS sites in the region are indicated.

Figure 3) The wind rose at Hans Island as represented in the 6-hourly: a) AWS observations; b) ERA5; c) ECOA and d) CARRA. The 10m winds were used to generate the ERA5, ECOA and CARRA wind roses. Data from January 1 2016-December 31 2019 excluding May-July 2016 was used.

Figure 4) The wind rose at Thule as represented in the 6-hourly: a) AWS observations; b) ERA5; c) ECOA and d) CARRA. The 10m winds were used to generate the ERA5, ECOA and CARRA wind roses. Data from January 1 2016-December 31 2019.

Figure 5) Mean and extreme 10m windspeed (m/s) for the Nares Strait region. The mean windspeed as represented in the: a) ERA5 ; b) ECOA and c) CARRA. The 95th percentile windspeed as represented in the: d) ERA5 ; e) ECOA and f) CARRA. In a)-c), the contour represents the 6 m/s isocontour. In d)-f), the contours represent the 14 and 22 m/s isocontours. Data from January 1 2016-December 31 2019.

Figure 6) The composite sea-level pressure (contours-mb), the 10m wind (vectors-m/s) and the 10 m windspeed (shading-m/s) for events where the CARRA 10m windspeed exceeded the 95th percentile value at the western Smith Sound location ('+') or at the eastern Smith Sound location (*). Results are shown for the: a) ERA5 at the western Smith Sound location ; b) ECOA at the western Smith Sound location; c) CARRA at the western Smith Sound location and d)) CARRA at the eastern Smith Sound location. In c) and d), the white contour represents the 23 m/s isocontour. Data from January 1 2016-December 31 2019.

Figure 7) One-point correlation maps showing the correlation between the 10m windspeed at Alert and at other gridpoints as represented in the: a) ERA5 ; b) ECOA and c) CARRA. Data from January 1 2016-December 31 2019.

Figure 8) One-point correlation maps showing the correlation between the 10m windspeed at Hans Island and at other gridpoints as represented in the: a) ERA5 ; b) ECOA and c) CARRA. Data from January 1 2016-December 31 2019.

Figure 9) One-point correlation maps showing the correlation between the 10m windspeed at western Smith Sound 95th percentile windspeed maxima and at other gridpoints as represented in the: a) ERA5 ; b) ECOA and c) CARRA. Data from January 1 2016-December 31 2019.

Table 1. Statistics of the comparison of the observed and model windspeeds along Nares Strait. For Hans Island, the comparison is also made for the 100m winds. For the bias error, the root mean square error is shown. Data from January 1 2016-December 31 2019.

References

Barber, D. G., Hanesiak, J. M., Chan, W., & Piwowar, J. (2001). Sea-ice and meteorological conditions in Northern Baffin Bay and the North Water polynya between 1979 and 1996. *Atmosphere-Ocean, 39*(3), 343-359. http://dx.doi.org/10.1080/07055900.2001.9649685

Barstad, I., & Grønås, S. (2005). Southwesterly flows over southern Norway—mesoscale sensitivity to large-scale wind direction and speed. *Tellus A: Dynamic Meteorology and Oceanography, 57*(2), 136-152. https://doi.org/10.3402/tellusa.v57i2.14627

Bengtsson, L., Andrae, U., Aspelien, T., Batrak, Y., Calvo, J., de Rooy, W., et al. (2017). The HARMONIE–AROME model configuration in the ALADIN–HIRLAM NWP system. *Monthly Weather Review, 145*(5), 1919-1935.

Bessels, E. (1876). Scientific Results of the United States Arctic Expedition, Steamer Polaris. *CF Hall Commanding. Vol. 1: Physical Observations*.

Bromwich, D. H., Cassano, J. J., Klein, T., Heinemann, G., Hines, K. M., Steffen, K., & Box, J. E. (2001). Mesoscale modeling of katabatic winds over Greenland with the Polar MM5. *Monthly Weather Review, 129*(9), 2290-2309.

Bromwich, D. H., Wilson, A., Bai, L.-S., Moore, G. W. K., & Bauer, P. (2015). A comparison of the regional Arctic System Reanalysis and the global ERA-Interim Reanalysis for the Arctic. *Quarterly Journal of the Royal Meteorological Society, 142*(695), 644-658.

De Benedetti, M., & Moore, G. (2020). Impact of model resolution on the representation of the wind speed field: An example from the United Kingdom. *Quarterly Journal of the Royal Meteorological Society, 146*(726), 367-379.

Dickson, R., Lazier, J., Meincke, J., Rhines, P., & Swift, J. (1996). Long-term coordinated changes in the convective activity of the North Atlantic. *Progress in Oceanography, 38*(3), 241-295. https://www.sciencedirect.com/science/article/pii/S0079661197000025

Dickson, R. R., Meincke, J., Malmberg, S.-A., & Lee, A. J. (1988). The "great salinity anomaly" in the Northern North Atlantic 1968–1982. *Progress in Oceanography, 20*(2), 103-151. https://www.sciencedirect.com/science/article/pii/0079661188900493

Dulière, V., Zhang, Y., & Salathé Jr, E. P. (2011). Extreme precipitation and temperature over the US Pacific Northwest: A comparison between observations, reanalysis data, and regional models. *Journal of Climate, 24*(7), 1950-1964.

Dumont, D., Gratton, Y., & Arbetter, T. E. (2010). Modeling Wind-Driven Circulation and Landfast Ice-Edge Processes during Polynya Events in Northern Baffin Bay. *Journal of Physical Oceanography, 40*(6), 1356-1372. https://doi.org/10.1175/2010JPO4292.1

Falkner, K. K., Melling, H., Münchow, A. M., Box, J. E., Wohlleben, T., Johnson, H. L., et al. (2011). Context for the recent massive Petermann Glacier calving event. *Eos, Transactions American Geophysical Union, 92*(14), 117-118.

Godske, C. L. B. V. B. V. (1957). Dynamic meteorology and weather forecasting. http://books.google.com/books?id=mTIXAQAAMAAJ

Greely, A. (1888). *Proceedings of the United States Expedition to Lady Franklin Bay, Grinnell Land* (Vol. 1). Washington: Government Printing Office.

Grivault, N., Hu, X., & Myers, P. G. (2018). Impact of the surface stress on the volume and freshwater transport through the Canadian Arctic Archipelago from a high-resolution numerical simulation. *Journal of Geophysical Research: Oceans, 123*(12), 9038-9060.

Gutjahr, O., & Heinemann, G. (2018). A model-based comparison of extreme winds in the Arctic and around Greenland. *International Journal of Climatology, 38*(14), 5272-5292.

Hayes, I. I. (1867). Physical observations in the Arctic Seas. *Smithsonian Contributions to Knowledge, 15(196)*, 248-549.

Heinemann, G. (2018). An Aircraft-Based Study of Strong Gap Flows in Nares Strait, Greenland. *Monthly Weather Review, 146*(11), 3589-3604.

Hersbach, H., Bell, B., Berrisford, P., Hirahara, S., Horányi, A., Muñoz-Sabater, J., et al. (2020). The ERA5 global reanalysis. *Quarterly Journal of the Royal Meteorological Society, 146*(730), 1999-2049.

Holm, E. V., Forbes, R., Lang, S., Magnusson, L., & Malardel, S. (2016). New model cycle brings higher resolution *ECMWF Newsletter, 147*.

Ingram, R. G., Bâcle, J., Barber, D. G., Gratton, Y., & Melling, H. (2002). An overview of physical processes in the North Water. *Deep Sea Research Part II: Topical Studies in Oceanography, 49*(22), 4893-4906. http://www.sciencedirect.com/science/article/pii/S0967064502001698

Jackson, J. M., Lique, C., Alkire, M., Steele, M., Lee, C. M., Smethie, W. M., & Schlosser, P. (2014). On the waters upstream of Nares Strait, Arctic Ocean, from 1991 to 2012. *Continental Shelf Research, 73*, 83-96.

Kirillov, S., Babb, D. G., Komarov, A. S., Dmitrenko, I., Ehn, J. K., Worden, E., et al. (2021). On the Physical Settings of Ice Bridge Formation in Nares Strait. *Journal of Geophysical Research: Oceans, 126*(8).

Kohnemann, S. H. E., & Heinemann, G. (2021). A climatology of wintertime low-level jets in Nares Strait. *Polar Research, 40*.

Kozo, T. L. (1991). The Hybrid Polynya At The Northern End Of Nares Strait. *Geophysical Research Letters, 18*(11), 2059-2062. <Go to ISI>://A1991GP75500033

Kwok, R., Toudal Pedersen, L., Gudmandsen, P., & Pang, S. S. (2010). Large sea ice outflow into the Nares Strait in 2007. *Geophysical Research Letters, 37*(3), n/a-n/a. http://dx.doi.org/10.1029/2009GL041872

Melling, H. (2011). The Best Laid Schemes: A Nares Strait Adventure. *Oceanography, 24*(3), 124-125.

Moore, G. (2016). The March 1972 northwest Greenland windstorm: evidence of downslope winds associated with a trapped lee wave. *Quarterly Journal of the Royal Meteorological Society, 142*(696), 1428-1438.

Moore, G., Bromwich, D. H., Wilson, A. B., Renfrew, I., & Bai, L. (2016). Arctic System Reanalysis improvements in topographically forced winds near Greenland. *Quarterly Journal of the Royal Meteorological Society, 142*(698), 2033-2045.

Moore, G., Howell, S. E. L., Brady, M., Xu, X., & McNeil, K. (2021). Anomalous collapses of Nares Strait ice arches leads to enhanced export of Arctic sea ice. *Nature Communications, 12*(1), 1-8.

Moore, G., & Pickart, R. S. (2012). Northern Bering Sea tip jets. *Geophysical Research Letters, 39*(8).

Moore, G., Renfrew, I., Harden, B., & Mernild, S. (2015). The impact of resolution on the representation of southeast Greenland barrier winds and katabatic flows. *Geophysical Research Letters, 42*(8), 3011-3018.

Moore, G., Schweiger, A., Zhang, J., & Steele, M. (2019). Spatiotemporal variability of sea ice in the arctic's last ice area. *Geophysical Research Letters, 46*(20), 11237-11243.

Moore, G. W. K. (2021). Impact of model resolution on the representation of the wind field along Nares Strait. *Scientific Reports, 11*.

Moore, G. W. K., & Våge, K. (2018). Impact of model resolution on the representation of the air–sea interaction associated with the North Water Polynya. *Quarterly Journal of the Royal Meteorological Society, 144*(714), 1474-1489. https://rmets.onlinelibrary.wiley.com/doi/abs/10.1002/qj.3295

Nutt, D. C. (1966). The drift of ice island WH-5. *Arctic*, 244-262.

Oltmanns, M., Straneo, F., Moore, G., & Mernild, S. (2014). Strong downslope wind events in Ammassalik, southeast Greenland. *Journal of Climate, 27*(3), 977-993.

Overland, J. E. (1984). Scale Analysis of Marine Winds in Straits and along Mountainous Coasts. *Monthly Weather Review, 112*(12), 2530-2534. https://doi.org/10.1175/1520-0493(1984)112<2530:SAOMWI>2.0.CO;2

Petersen, G. N., Renfrew, I., & Moore, G. (2009). An overview of barrier winds off southeastern Greenland during the Greenland Flow Distortion experiment. *Quarterly Journal of the Royal Meteorological Society: A journal of the atmospheric sciences, applied meteorology and physical oceanography, 135*(645), 1950-1967.

Samelson, R. M., Agnew, T., Melling, H., & Münchow, A. (2006). Evidence for atmospheric control of sea-ice motion through Nares Strait. *Geophysical Research Letters, 33*(2), n/a-n/a. http://dx.doi.org/10.1029/2005GL025016

Samelson, R. M., & Barbour, P. L. (2008). Low-Level Jets, Orographic Effects, and Extreme Events in Nares Strait: A Model-Based Mesoscale Climatology. *Monthly Weather Review, 136*(12), 4746-4759. https://doi.org/10.1175/2007MWR2326.1

Sharp, J., & Mass, C. F. (2004). Columbia Gorge gap winds: Their climatological influence and synoptic evolution. *Weather and Forecasting, 19*(6), 970-992.

Shokr, M. E., Wang, Z., & Liu, T. (2020). Sea ice drift and arch evolution in the Robeson Channel using the daily coverage of Sentinel-1 SAR data for the 2016–2017 freezing season. *The Cryosphere, 14*(11), 3611-3627. https://tc.copernicus.org/articles/14/3611/2020/

Smith, R. B. (1985). On severe downslope winds. *Journal of Atmospheric Sciences, 42*(23), 2597-2603.

Stansfield, J. R. (1972). The Severe Arctic Storm of 8–9 March 1972 at Thule Air Force Base, Greenland. *Weatherwise, 25*(5), 228-232. https://doi.org/10.1080/00431672.1972.9931607

Steffen, K. (1985). Warm water cells in the North Water, Northern Baffin Bay during winter. *Journal of Geophysical Research: Oceans, 90*(C5), 9129-9136. http://dx.doi.org/10.1029/JC090iC05p09129

Tollinger, M., Gohm, A., & Jonassen, M. O. (2019). Unravelling the March 1972 northwest Greenland windstorm with high-resolution numerical simulations. *Quarterly Journal of the Royal Meteorological Society, 145*(725), 3409-3431.

van As, D., Fausto, R. S., Steffen, K., & Promice project team. (2015). Katabatic winds and piteraq storms: observations from the Greenland ice sheet. *GEUS Bulletin, 31*, 83-86. https://geusbulletin.org/index.php/geusb/article/view/4669

Wallace, J. M., & Gutzler, D. S. (1981). Teleconnections in the geopotential height field during the Northern Hemisphere winter. *Monthly Weather Review, 109*(4), 784-812.

Wilkinson, J., Gudmandsen, P., Hanson, S., Saldo, R., & Samelson, R. (2009). Hans Island: Meteorological data from an international borderline. *Eos, Transactions American Geophysical Union, 90*(22), 190-191.

Wright, J. (1940). South-east Ellesmere Island. *The Geographical Journal, 95*(4), 278-291.

Yang, X. (2020). *C3S Arctic regional reanalysis – Full system documentation*. Retrieved from

	Slope			Correlation Coefficient			Root Mean Square Error			Bias Error		
	ERA5	ECOA	CARRA	ERA5	ECOA	CARRA	ERA5	ECOA	CARRA	ERA5	ECOA	CARRA
Alert	0.38	0.52	0.70	0.75	0.76	0.82	2.64	2.39	2.12	-0.63	0.07	0.12
Hans Island	0.36	0.77	0.81	0.77	0.87	0.87	4.21	2.15	2.19	-2.84	-0.01	-0.41
Hans Island 100m	0.51	0.98	0.96	0.75	0.87	0.96	3.11	3.36	3.34	-1.04	2.28	2.16
Kitisissut	0.75	0.76	0.80	0.77	0.80	0.82	2.58	2.43	2.27	0.26	0.52	-0.15
Qaanaaq	0.22	0.34	0.79	0.54	0.59	0.76	2.66	2.44	2.23	-0.62	-0.16	0.50
Thule	0.43	0.43	0.75	0.73	0.71	0.74	2.44	3.01	2.55	-1.00	-1.95	-1.02
mean*	0.44	0.63	0.80	0.72	0.77	0.83	2.94	2.63	2.45	1.35	1.25	1.01

Table 1. Statistics of the comparison of the observed and model wind speeds along Nares Strait. For Hans Island, the comparison is also made for the 100m winds. For the bias error, the root mean square error is shown. Data from January 1 2016-December 31 2019.

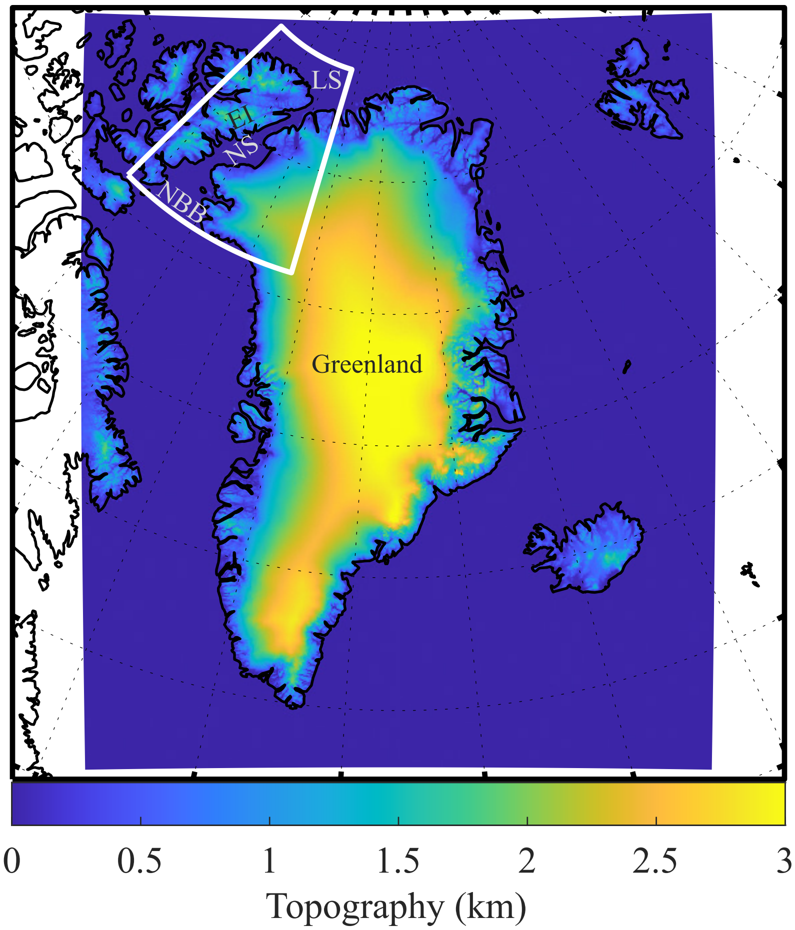

Figure 1) Topography (km) from the western domain of the Copernicus Arctic Regional Reanalysis. The Nares Strait region is indicated by the white polygon. The locations of the Lincoln Sea (LS), Ellesmere Island (EI), Nares Strait (NS) and northern Baffin Bay (NBB) are indicated.

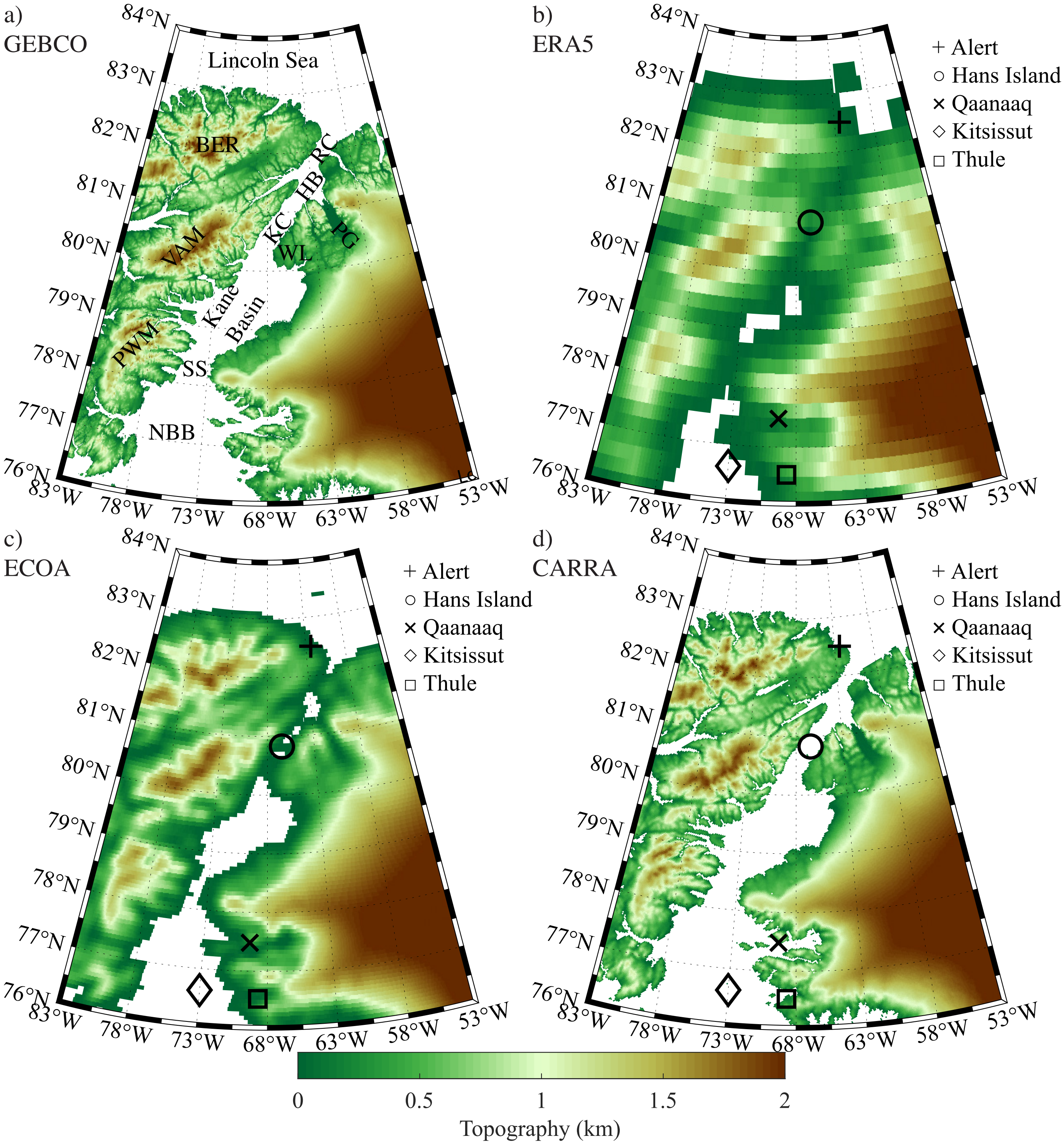

Figure 2) Topography (km) of the Nares Strait region as represented in the: a) GEBCO DEM; b) ERA5, c) ECOA and d) CARRA. In a) the abbreviations for locations along the strait are: northern Baffin Bay (NBB); Smith Sound (SS); Kennedy Channel (KC); Hall Basin (HB); Robeson Channel (RC), Washington Land (WL) and the Petermann Glacier (PG). Regions of high topography on Ellesmere Island, the Prince of William Mountains (PWM); the Victoria and Albert Mountains (VAM) and the British Empire Range (BER) are indicated. In b)-d), the locations of AWS sites in the region are indicated.

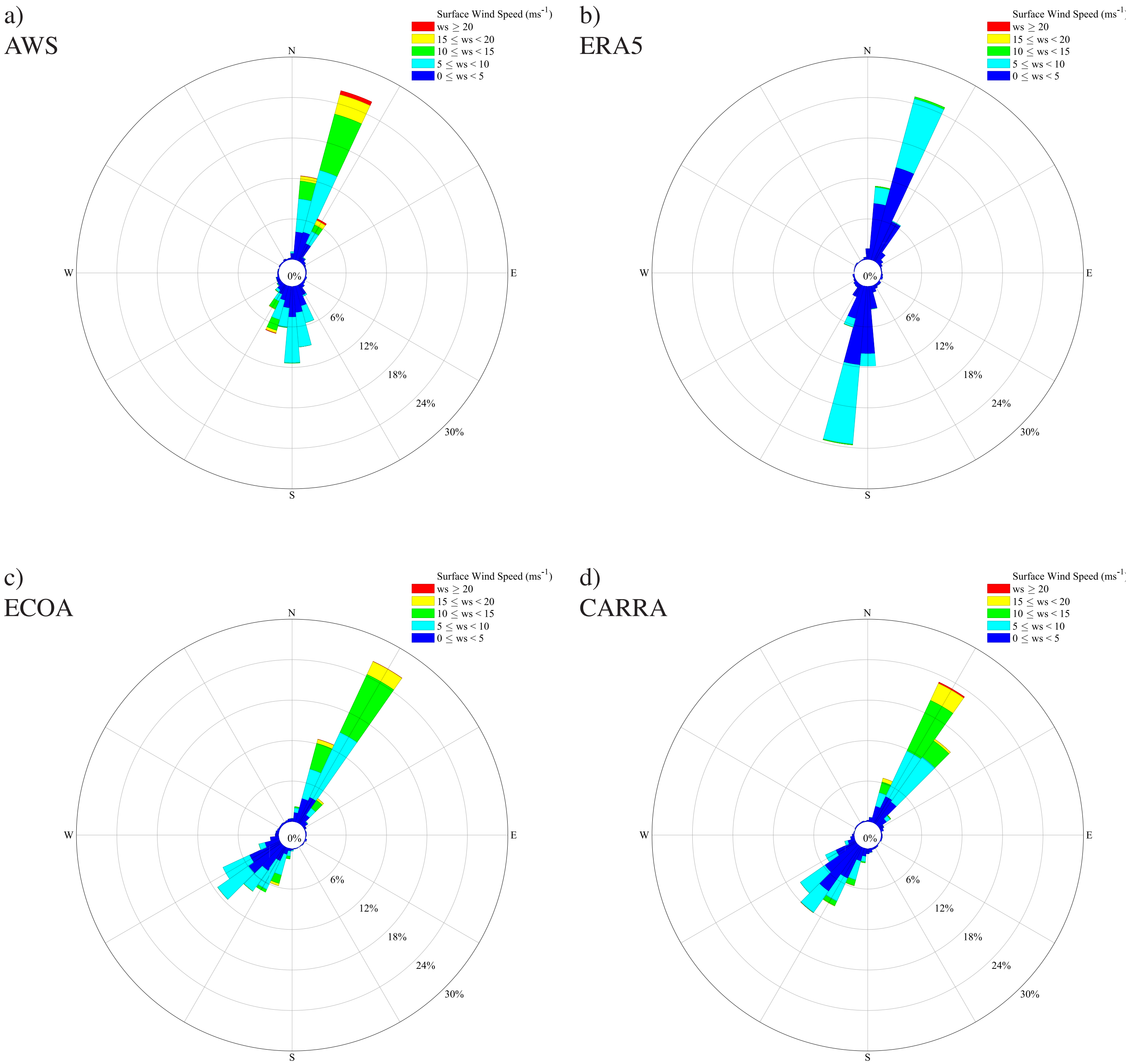

Figure 3) The wind rose at Hans Island as represented in the 6-hourly: a) AWS observations; b) ERA5; c) ECOA and d) CARRA. The 10m winds were used to generate the ERA5, ECOA and CARRA wind roses. Data from January 1 2016-December 31 2019 excluding May-July 2016 was used.

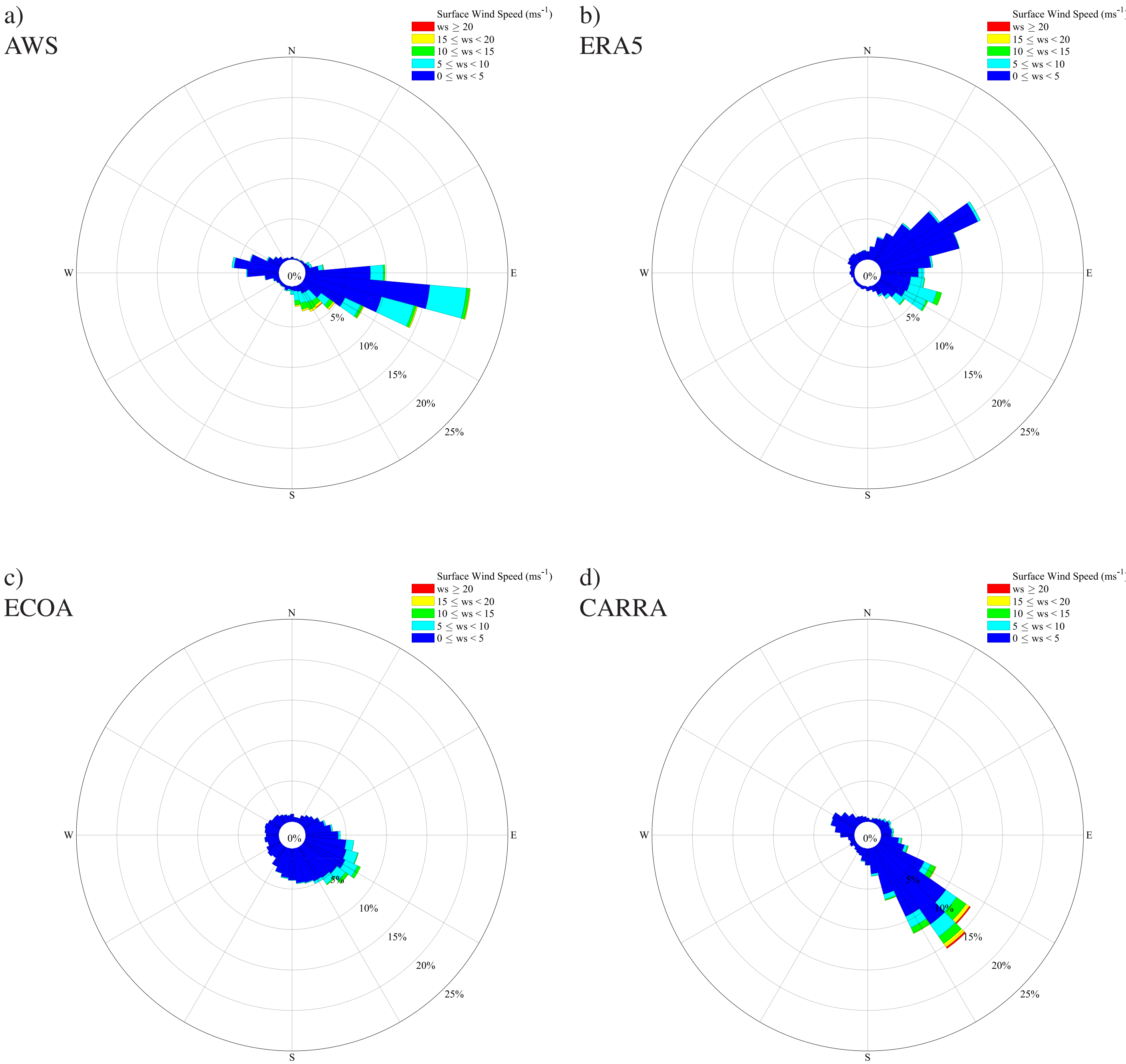

Figure 4) The wind rose at Thule as represented in the 6-hourly: a) AWS observations; b) ERA5; c) ECOA and d) CARRA. The 10m winds were used to generate the ERA5, ECOA and CARRA wind roses. Data from January 1 2016-December 31 2019.

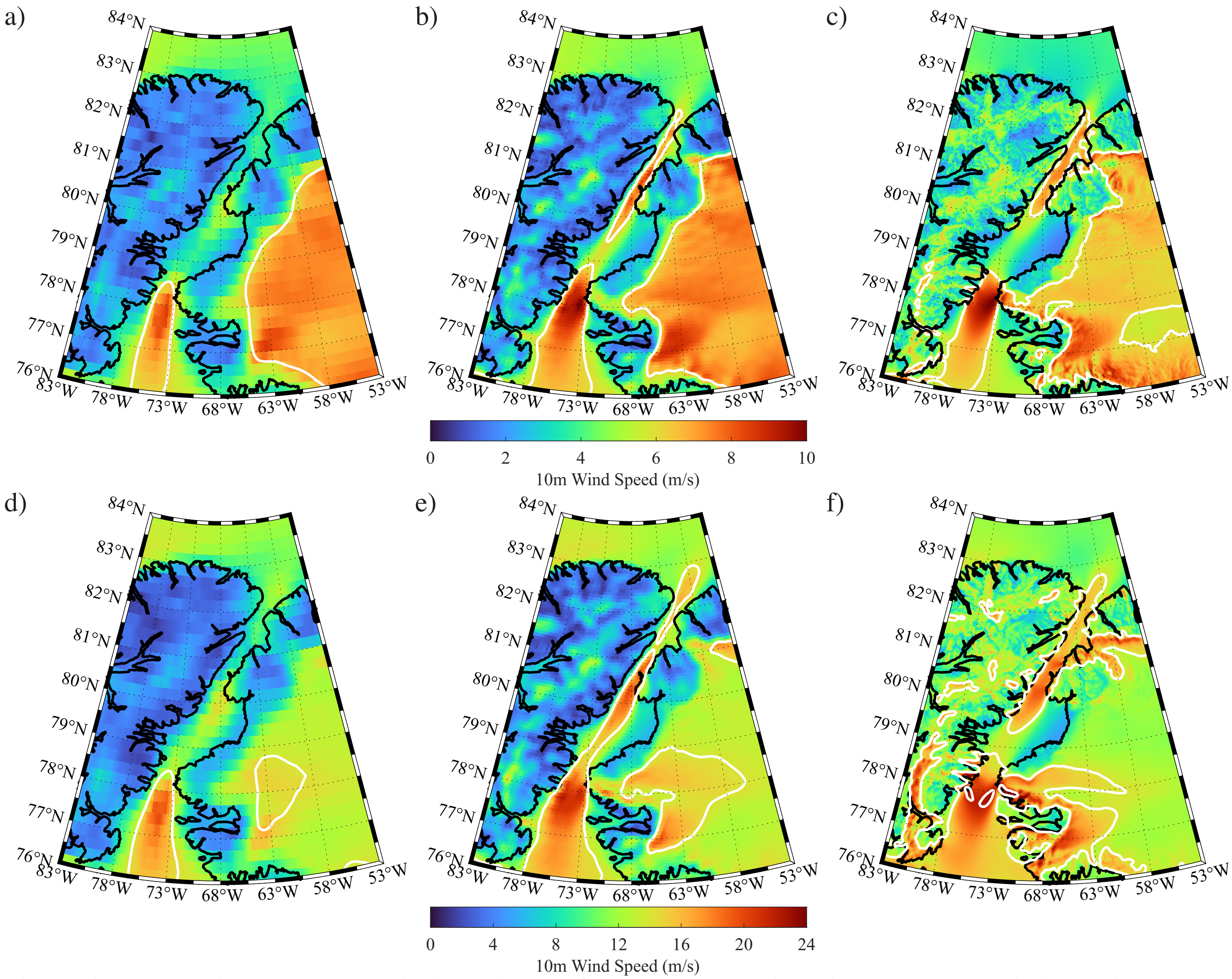

Figure 5) Mean and extreme 10m wind speed (m/s) for the Nares Strait region. The mean wind speed as represented in the: a) ERA5 ; b) ECOA and c) CARRA. The 95th percentile wind speed as represented in the: d) ERA5 ; e) ECOA and f) CARRA. In a)-c), the contour represents the 6 m/s isocontour. In d)-f), the contours represent the 14 and 22 m/s isocontours. Data from January 1 2016-December 31 2019.

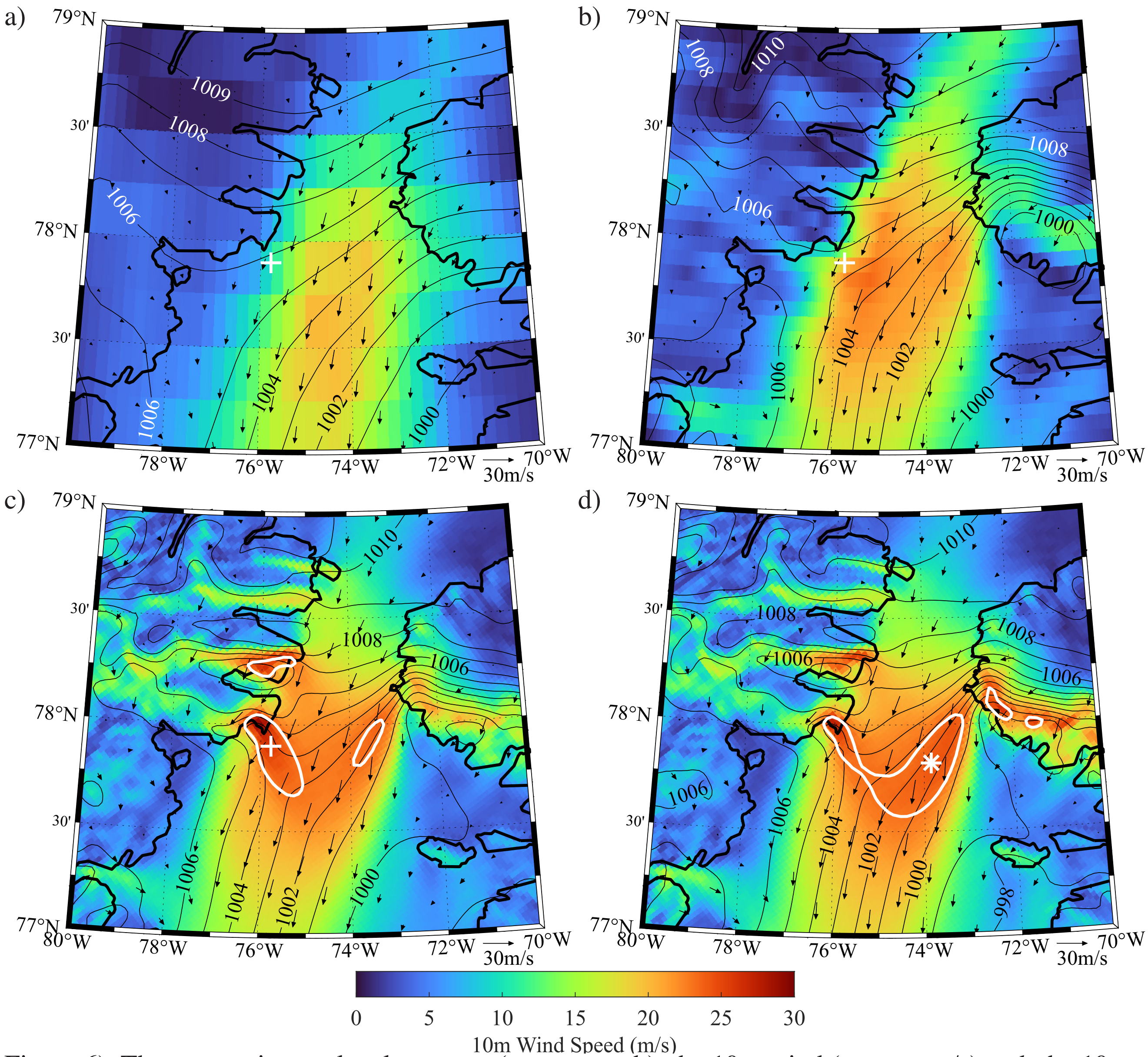

Figure 6) The composite sea-level pressure (contours-mb), the 10m wind (vectors-m/s) and the 10 m wind speed (shading-m/s) for events where the CARRA 10m wind speed exceeded the 95th percentile value at the western Smith Sound location ('+') or at the eastern Smith Sound location (*). Results are shown for the: a) ERA5 at the western Smith Sound location ; b) ECOA at the western Smith Sound location; c) CARRA at the western Smith Sound location and d)) CARRA at the eastern Smith Sound location. In c) and d), the white contour represents the 23 m/s isocontour. Data from January 1 2016-December 31 2019.

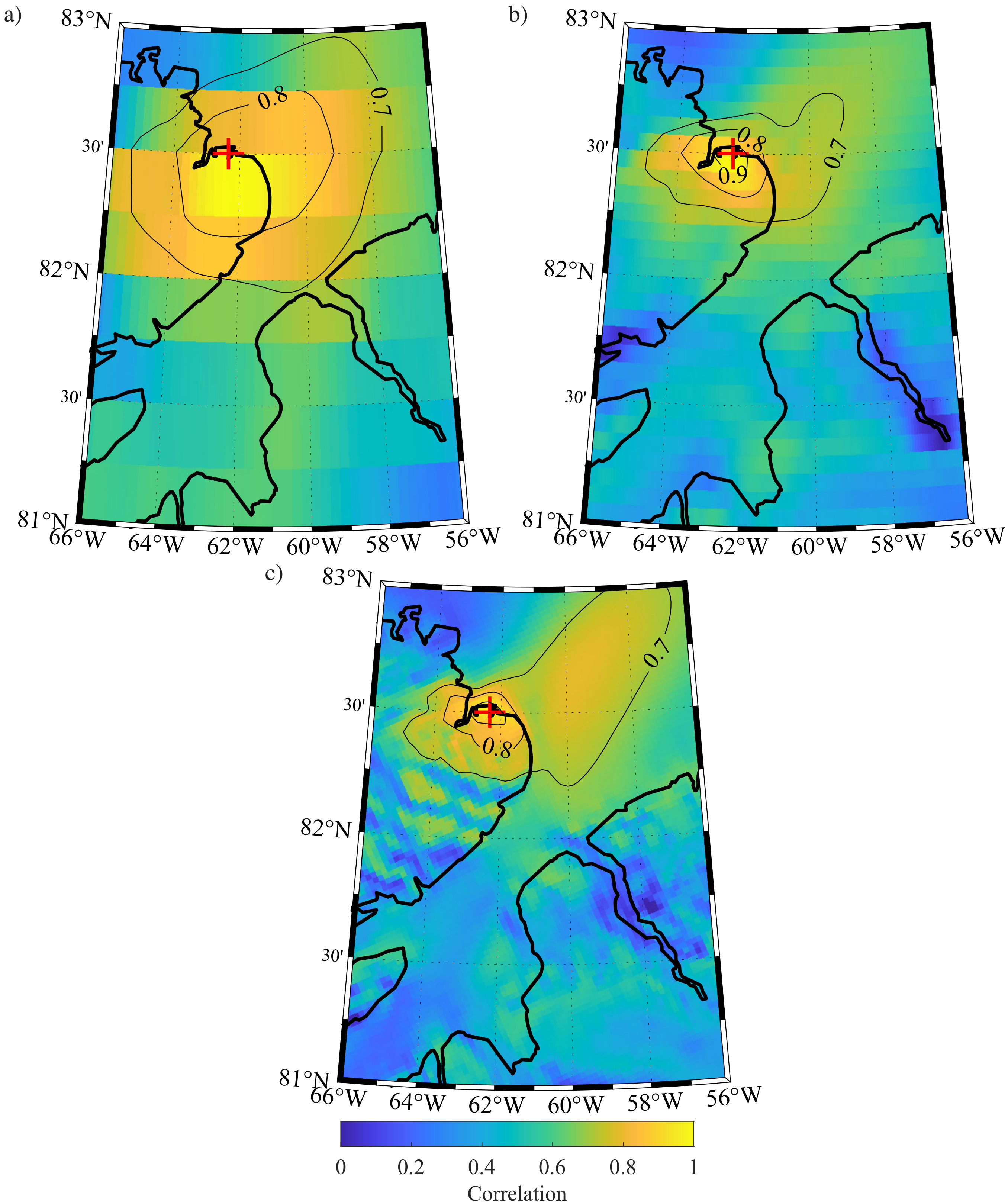

Figure 7) One-point correlation maps showing the correlation between the 10m wind speed at Alert and at other gridpoints as represented in the: a) ERA5 ; b) ECOA and c) CARRA. Data from January 1 2016-December 31 2019.

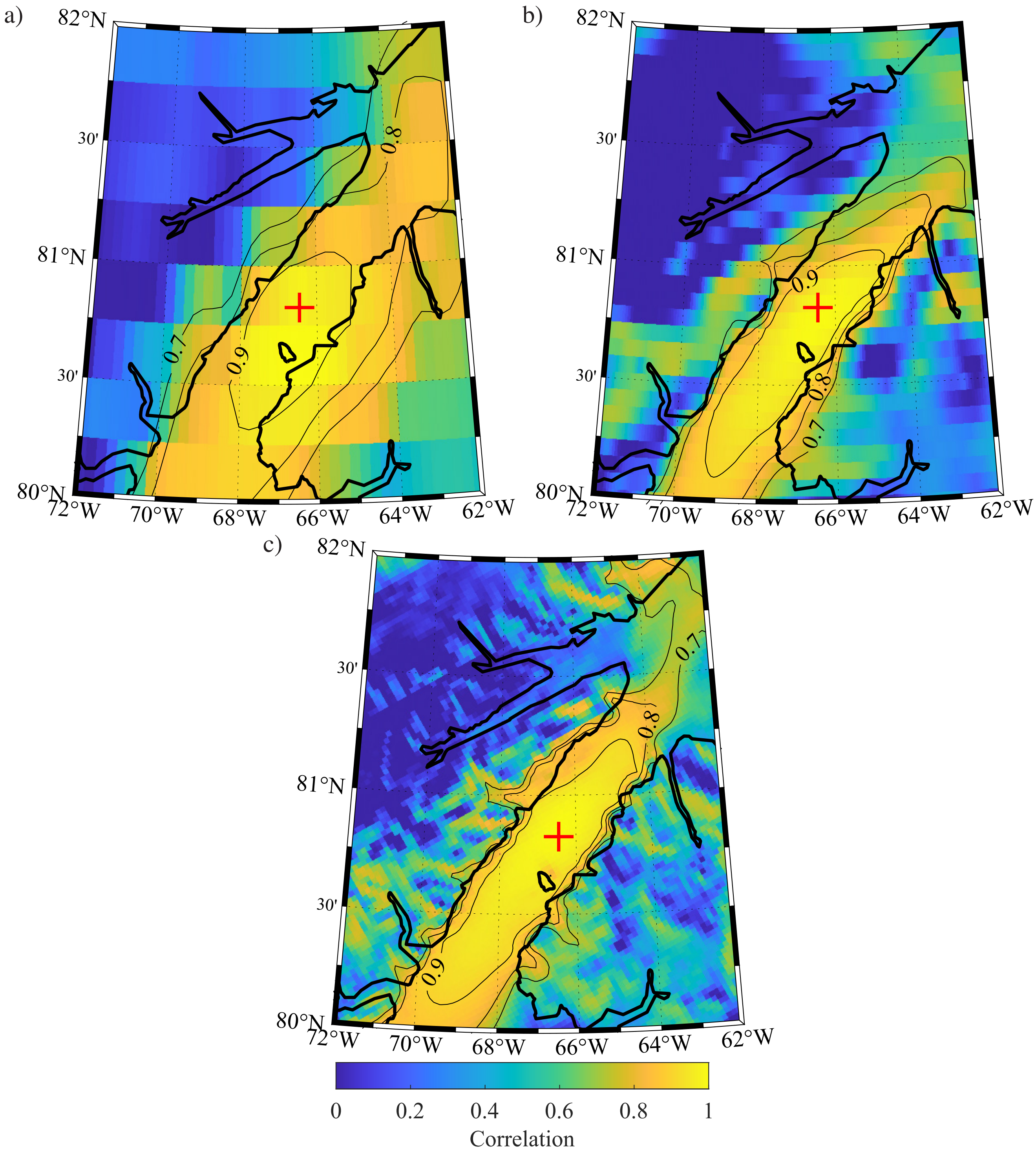

Figure 8) One-point correlation maps showing the correlation between the 10m wind speed at Hans Island and at other gridpoints as represented in the: a) ERA5 ; b) ECOA and c) CARRA. Data from January 1 2016-December 31 2019.

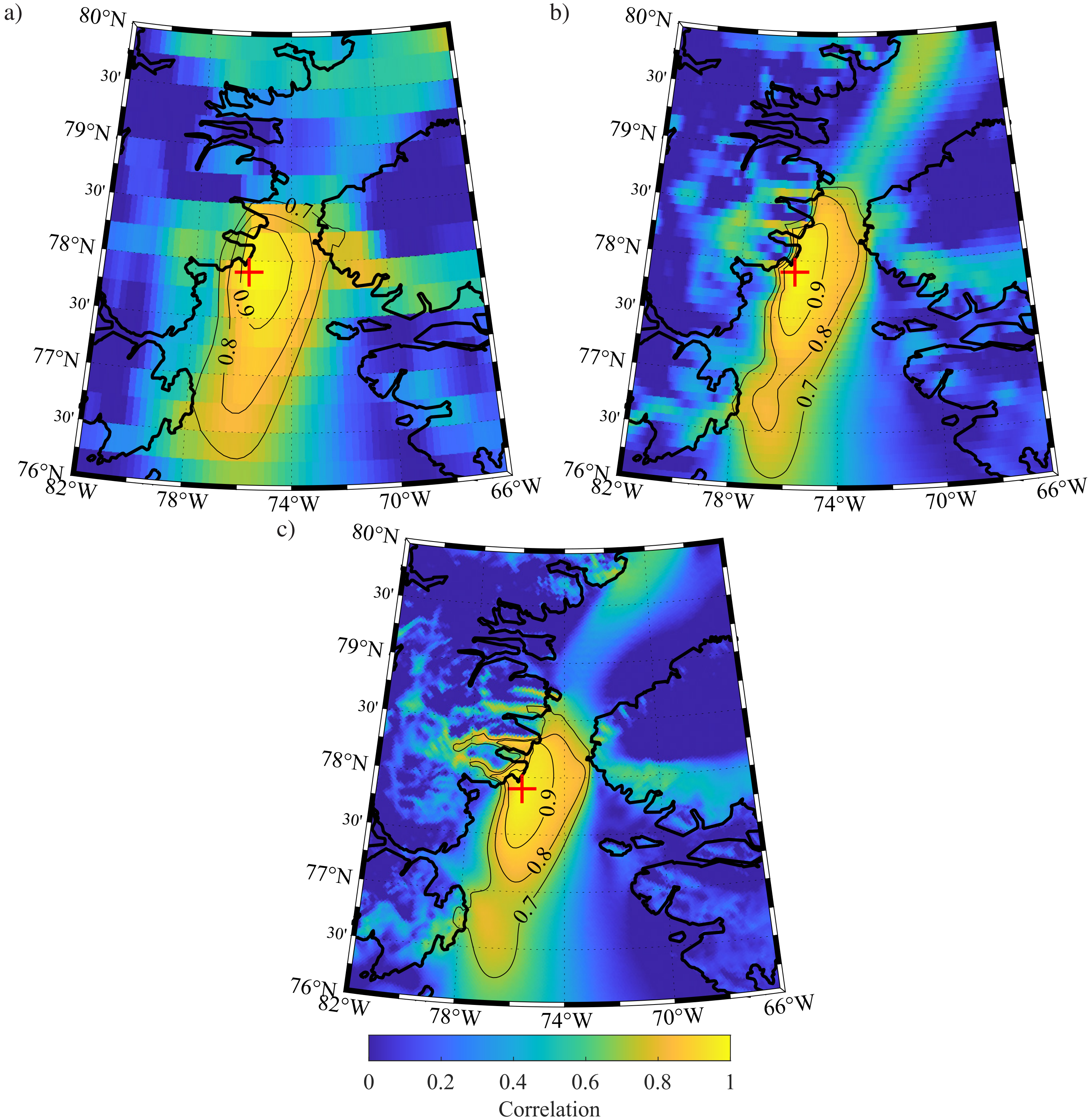

Figure 9) One-point correlation maps showing the correlation between the 10m wind speed at western Smith Sound 95th percentile wind speed maxima and at other gridpoints as represented in the: a) ERA5 ; b) ECOA and c) CARRA. Data from January 1 2016-December 31 2019.